Complexity of human walking: the attractor complexity index is sensitive to gait synchronization with visual and auditory cues

Philippe Terrier[1,2,3]

[1]Haute-Ecole Arc Santé, HES-SO University of Applied Sciences and Arts Western Switzerland, Neuchâtel, Switzerland
[2] Department of Thoracic and Endocrine Surgery, University Hospitals of Geneva, Geneva, Switzerland
[3]Clinique romande de réadaptation SUVA, Sion, Switzerland

Corresponding author:
Philippe Terrier
Haute Ecole Arc Santé
Espace de l'Europe 11, CH-2000 Neuchâtel, Switzerland
Email address: Philippe.terrier@he-arc.ch

Abstract

Background. During steady walking, gait parameters fluctuate from one stride to another with complex fractal patterns and long-range statistical persistence. When a metronome is used to pace the gait (sensorimotor synchronization), long-range persistence is replaced by stochastic oscillations (anti-persistence). Fractal patterns present in gait fluctuations are most often analyzed using detrended fluctuation analysis (DFA). This method requires the use of a discrete times series, such as intervals between consecutive heel strikes, as an input. Recently, a new nonlinear method, the attractor complexity index (ACI), has been shown to respond to complexity changes like DFA, while being computed from continuous signals without preliminary discretization. Its use would facilitate complexity analysis from a larger variety of gait measures, such as body accelerations. The aim of this study was to further compare DFA and ACI in a treadmill experiment that induced complexity changes through sensorimotor synchronization.

Methods. Thirty-six healthy adults walked 30 minutes on an instrumented treadmill under three conditions: no cueing, auditory cueing (metronome walking), and visual cueing (stepping stones). The center-of-pressure trajectory was discretized into time series of gait parameters, after which a complexity index (scaling exponent alpha) was computed via DFA. Continuous pressure position signals were used to compute the ACI. Correlations between ACI and DFA were then analyzed. The predictive ability of DFA and ACI to differentiate between cueing and no-cueing conditions was assessed using regularized logistic regressions and areas under the receiver operating characteristic curves (AUC).

Results. DFA and ACI were both significantly different among the cueing conditions. DFA and ACI were correlated (Pearson's r = 0.86). Logistic regressions showed that DFA and ACI could differentiate between cueing/no cueing conditions with a high degree of confidence (AUC = 1.00 and 0.97, respectively).

Conclusion. Both DFA and ACI responded similarly to changes in cueing conditions and had comparable predictive power. This support the assumption that ACI could be used instead of DFA to assess the long-range complexity of continuous gait signals. However, future studies are required to investigate the theoretical relationships between DFA and ACI.

Introduction

Gait is a stereotyped sequence of movements that enable human beings to move through their environment. A fluid and stable gait requires the complex coordination of dozens of muscles controlling multiple joints. Biomechanical and energy constraints limit the range of gait movements to a narrow window (Holt et al., 1995); for example, at a preferred walking speed, step length and step time vary by only a few percent (Terrier, Turner & Schutz, 2005). It was previously thought that these small variations were random noise introduced by residual

60 neuromuscular inaccuracies; however, after studying the structure of gait variability among
61 hundreds of consecutive strides, it was observed that stride-to-stride fluctuations were not totally
62 random but instead exhibited a fractal pattern (Hausdorff et al., 1995). Fractal fluctuations in
63 time series produced by living beings have been deemed to be a signature of their complex
64 internal organization and of the feedback loops needed to adapt behaviors to environmental
65 changes (Goldberger et al., 2002; West, 2013). Accordingly, physiological time series most often
66 exhibit scaling properties and statistical persistence. Regarding human walking, the complex
67 fluctuations in stride intervals, stride speeds, and stride lengths exhibit fractal patterns with
68 inverse power-law memory (Hausdorff et al., 1995; Terrier, Turner & Schutz, 2005); that is, a
69 change occurring at a given gait cycle can potentially influence another cycle dozens of steps
70 later.
71   The fractal pattern of gait fluctuations can be disrupted by sensorimotor synchronization. It is
72 possible for humans to synchronize their stepping with external rhythmic cues, such as walking
73 in time with a musical rhythm (auditory cueing). In such cases, stride-to-stride fluctuations
74 become anti-persistent; that is, stride intervals tend to oscillate stochastically around the imposed
75 pace (Terrier, Turner & Schutz, 2005; Delignières & Torre, 2009; Sejdić et al., 2012; Choi et al.,
76 2017). In other words, a long stride interval has a higher probability of being followed by a short
77 stride interval. Similarly, time series of stride speeds are anti-persistent in treadmill walking, in
78 which a constant speed is imposed by the treadmill belt (Dingwell & Cusumano, 2010). The
79 fractal pattern of stride speeds can be restored using self-paced treadmills, in which the belt
80 speed is dynamically controlled by the walking subjects (Choi et al., 2017). In treadmill
81 experiments, if an additional instruction of gait synchronization is superimposed on the task of
82 walking at the belt speed, a generalized anti-persistent pattern is then observed (Terrier & Dériaz,
83 2012; Roerdink et al., 2015; Choi et al., 2017). This phenomenon exists both when
84 synchronizing stride intervals to a metronome (auditory cueing), and when aligning step lengths
85 to visual cues projected onto the treadmill belt (visual cueing) (Terrier, 2016).
86   In 2010, Dingwell and Cusumano hypothesized that the emergence of anti-persistence was
87 linked to the degree of voluntary control dedicated to the gait. They suggested that, during a
88 normal gait, deviations go uncorrected and can persist across consecutive strides (under-
89 correction). In contrast, in paced walking, deviations are followed by rapid corrections that lead
90 to anti-persistence (over-correction). This "tight control" hypothesis has been supported by other
91 studies (Roerdink et al., 2015; Bohnsack-McLagan, Cusumano & Dingwell, 2016). Earlier this
92 year, Roerdink et al. further demonstrated that the degree of anti-persistence can be modulated
93 by constraining the maneuverability range on a treadmill (Roerdink et al., 2019). In short,
94 characterizing the noise structure of gait variability helps us to better understand gait control;
95 among other things, it can provide information about whether a gait is highly controlled or more
96 automated. In addition, cued walking has important applications for rehabilitation in gait
97 disorders (Yoo & Kim, 2016; Pereira et al., 2019).
98   Detrended fluctuation analysis (DFA) is typically the preferred method to identify the
99 fluctuation structure in a time series of gait parameters. Introduced in 1995 by Hausdorff et al.,

100 DFA identifies the modification of a signal's variance at different time scales. DFA can unmask
101 underlying fluctuation structures that may be otherwise obscured by time series trends (Peng et
102 al., 1995). The presence of power-law scaling is determined through the scaling exponent alpha
103 (α); if the exponent is small ($\alpha < 0.5$), the fluctuations are deemed to be anti-persistent. Statistical
104 persistence corresponds to α values higher than 0.5 and an α value equal to 0.5 indicates a
105 random, uncorrelated noise (see Appendix B in Terrier & Dériaz [2013] for further information).
106   DFA requires a non-periodical, discrete time series as an input. Foot switches, i.e., pressure
107 sensitive insoles, can be used to detect heel strikes on the ground and can thus collect time series
108 of stride intervals (Hausdorff, Ladin & Wei, 1995; Sejdić et al., 2012; Almurad et al., 2018).
109 Several methods using the continuous measure of the positions of various body parts have also
110 been proposed: 1) high-accuracy GPS (Terrier, Turner & Schutz, 2005); 2) 3-D video analysis of
111 treadmill walking (Dingwell & Cusumano, 2010); and 3) an instrumented treadmill that records
112 the center-of-pressure trajectory (Terrier & Dériaz, 2012; Terrier, 2016; Roerdink et al., 2019).
113 These methods require a preliminary discretization of the position signals via minima/maxima
114 detection algorithms (Terrier & Schutz, 2005; Roerdink et al., 2008; Dingwell & Cusumano,
115 2010).
116   Other studies attempted to retrieve stride intervals from acceleration signals (Terrier &
117 Dériaz, 2011), but the correct discrimination of strides can be challenging. Accelerometers are
118 most often attached to the lower back for optimally assessing whole-body movements and for
119 enhancing the compliance in wearing a sensor over long periods of time. The dampening of
120 accelerations throughout the limbs can make difficult the detection of foot contacts, which are
121 required to compute stride durations (Terrier & Reynard, 2018). For example, a poor detection of
122 gait events leads to large errors when evaluating walking distance from trunk accelerations
123 (Lopez et al., 2008). Although solutions exist under optimal conditions (González et al., 2010), it
124 has been suggested that methods that do not require a preliminary detection of gait events could
125 be advantageous when studying pathological gaits with atypical acceleration signals (Riva et al.,
126 2013). A method that can analyze gait complexity from continuous signals may be useful in
127 ecological monitoring of pathological gaits (Terrier et al., 2017).
128   The discrete gait time series that are analyzed through DFA are fundamentally the output of a
129 continuous process. Indeed, gait control coordinates muscles and joints continuously during
130 successive gait cycles; this process generates stride intervals, stride lengths, and stride speeds as
131 outputs. It is questionable whether it is even possible to retrieve the fractal signature of long-
132 range stride fluctuations in a continuous signal that could capture both intra- and inter- stride gait
133 dynamics. In 2013, I hypothesized that an attractor that reflects short-term gait dynamics could
134 also contain information about long-term gait complexity (Terrier & Dériaz, 2013). In 2018, I
135 explored this hypothesis further (Terrier & Reynard, 2018): I proposed the use of a new gait
136 complexity index computed from continuous signals, which I named the attractor complexity
137 index (ACI).
138   ACI is a new term for long-term local dynamic stability (LDS)—also referred to as
139 divergence exponent or lambda (λ)—which was introduced by Dingwell et al. in 2000 (Dingwell

140   et al., 2000; Dingwell & Cusumano, 2000). This algorithm, based on Lyapunov exponents used
141   in chaos theory (Dingwell, 2006; Mochizuki & Aliberti, 2017), has been recommended to assess
142   gait stability and fall risk (Bruijn et al., 2013). LDS requires the construction of an attractor in
143   the phase space by means of time delay embedding of continuous signals, such as body
144   accelerations (Takens, 1981; Rosenstein, Collins & De Luca, 1993; Terrier & Dériaz, 2013).
145   LDS is defined as the divergence rate among attractor trajectories. The divergence rate can be
146   evaluated at different intervals, either immediately after the initial separation between adjacent
147   trajectories (short-term LDS) or several strides later (long-term LDS). In the years following
148   Dingwell's seminal articles, it became clear that long-term LDS was in fact not a good index for
149   predicting fall risk and gait stability (Bruijn et al., 2013), but that short-term LDS had better
150   properties for gait stability analysis, as shown in modeling studies (Su & Dingwell, 2007; Bruijn
151   et al., 2012).
152   Studies have shown that long-term LDS responded to various experimental conditions
153   independently of short-term LDS. In visually and mechanically destabilizing environments,
154   short-term and long-term LDS vary in opposite directions (McAndrew, Wilken & Dingwell,
155   2011). Similar results have been obtained when galvanic vestibular stimulation is used to impair
156   dynamic balance (van Schooten et al., 2011). Walking on a compliant surface decreases long-
157   term LDS, with no relevant effects on short-term LDS (Chang et al., 2010). Overall, an
158   accumulation of evidence supports the fact that long- and short-term LDS measure different
159   aspects of gait control, which may justify a change in the terminology to clearly differentiate
160   between them.
161   Given that long-term LDS is not a gait stability index, renaming it as ACI seems appropriate.
162   Indeed, as demonstrated through a modelling approach, ACI is highly sensitive to the noise
163   structure of stride intervals (Terrier & Reynard, 2018). More precisely, a low ACI is associated
164   with statistical anti-persistence, and a high ACI is associated with persistence. Furthermore, it
165   has been shown that when stride intervals are kept constant, divergence curves become flat after
166   only two strides (see Fig. 2 in Terrier & Reynard [2018]). Although additional theoretical work
167   is required to explore the causes of this sensitivity, it can be assumed that the complex gait
168   dynamic is reflected by wider boundaries in the attractor, which allows further long-term
169   divergence. In contrast, statistical anti-persistence signals a less complex gait dynamic, a more
170   restricted attractor, and therefore a lower long-term divergence rate. The fact that no divergence
171   is observed if stride intervals are kept constant further supports this hypothesis.
172   The objective of the present study was to confirm that ACI can be used to assess gait
173   complexity from continuous signals without preliminary discretization. In my 2018 study
174   (Terrier & Reynard, 2018), I hybridized acceleration signals with artificial signals to explore this
175   assumption. Here, in order to apply ACI to real signals, I computed both ACI and scaling
176   exponents (αs) from a center-of-pressure trajectory recorded in a treadmill experiment that
177   submitted participants to either visual or auditory cueing. I then explored the responsiveness of
178   ACI to the cueing conditions, as well as correlations between ACI and αs. The ability of ACI and
179   αs to predict cueing conditions was also assessed. The study also had two secondary objectives:

180   to test the appropriateness of different intervals for computing ACI, and to evaluate short-term
181   LDS's sensitivity to cueing.
182
183   **Materials & Methods**
184   **Data**
185   Data from a previous study were re-analyzed (Terrier, 2016). In summary, 36 individuals walked
186   for 30 min on an instrumented treadmill at their preferred speed. They were exposed to three
187   different conditions of 10 min duration each: 1) normal walking with no cueing; 2) walking
188   while synchronizing their gait cadence to an isochronous metronome (auditory cueing); and 3)
189   walking while targeting visually projected shapes with their feet (visual cueing).
190   **Ethics statement**
191   The present study is a re-analysis of an anonymized database and is not considered as a human
192   research needing authorization from an ethic committee. Consent was obtained for
193   anonymization and reuse. Please refer to the ethic statement in the original publication for further
194   information (Terrier, 2016).
195   **Data availability**
196   Individual data are available in a supplementary file. Raw signals are hosted on Figshare.
197   **Data processing**
198   For each condition, 1,000 steps (500 gait cycles) were recorded. The force platform embedded
199   into the treadmill recorded the position (Cartesian coordinates, anteroposterior [AP] and
200   mediolateral [ML] axes) of the center of pressure at a sampling rate of 500Hz. Based on the
201   detection of heel strikes in the anteroposterior (AP) signal, time series of stride time (ST), stride
202   length (SL) and stride speed (SS) were computed (Roerdink et al., 2008). Next, the noise
203   structure of stride-to-stride fluctuations were assessed with DFA (for in-depth descriptions of the
204   DFA algorithm, see Terrier, Turner & Schutz [2005] and Terrier & Dériaz [2012, 2013]; DFA
205   results—the scaling exponents α—are shown in Terrier [2016]). DFA was implemented with box
206   sizes ranging from 12 to 125 (i.e., N / 4) using the evenly spaced algorithm (Almurad &
207   Delignières, 2016).
208   The 500Hz signal from the AP and ML signals were then low-pass filtered (18Hz 12th order
209   Butterworth) and down-sampled to 100Hz. Raw 500-strides signals were resampled at a constant
210   number of 50,000 samples, i.e., 100 points per stride.
211   Computations of nonlinear indexes of gait stability (LDS) and complexity (ACI) were
212   implemented via the same methods as in previous studies that used Rosenstein's algorithm
213   (Rosenstein, Collins & De Luca, 1993; Terrier & Dériaz, 2013; Terrier & Reynard, 2015). High
214   dimensional attractors were built according to the delay-embedding theorem. The average mutual
215   information of each signal was used to assess the time delay (Fraser & Swinney, 1986). A
216   common dimension of five was determined with a global false nearest neighbor analysis
217   (Kennel, Brown & Abarbanel, 1992). Average divergence of the attractor was defined as
218   *avg(ln[$d_j(i)$])*, that is, the logarithm of the ith Euclidian distance *d* downstream of the jth pair of
219   nearest neighbors in the attractor, averaged over all pairs. Time was normalized by ST. Resulting

220   divergence curves are shown in Fig. 1. The exponential divergence rate, calculated as

221   *avg(ln[dj(i)]) / stride*, was evaluated with linear fits across several spans as follows: 0–0.5 stride

222   (LDS), 1–4 strides (ACI 1-4), 4–7 strides (ACI 4-7), and 7–10 strides (ACI 7-10). These spans

223   not only cover the classical range usually used for computing the long-range LDS (4-10), but

224   also cover spans closer to initial separation that have not been studied so far (1-4).

225   **Statistics**

226   Notched boxplots were used to depict the distribution of the individual results (Figs. 2 and 3).

227   Descriptive statistics (means and standard deviations [SD]) were computed for the ACIs (Table

228   1). LDS statistics can be found in the supplementary file. Fig. 4 shows the effect sizes (Hedges'

229   *g*) of the differences between conditions (i.e., auditory cueing minus no cueing, and visual cueing

230   minus no cueing), as well as Bonferroni corrected 95 % confidence intervals.

231   The correlations among the variables are illustrated in Fig. 5 through scatter plots and linear

232   fits. Pearson's correlation coefficients (*r*) and null hypotheses for a null correlation coefficient

233   were also assessed.

234   Least absolute shrinkage and selection operator LASSO (Tibshirani, 1996) and logistic

235   regressions were used to assess the extents to which DFA, LDS and ACI could differentiate

236   between the cueing (auditory and visual) and no-cueing conditions. The LASSO algorithm had

237   the advantage of regularizing the fit for lower overfitting and of selecting the most important

238   predictors. The dependent binary variable was coded as no-cueing = 1 (36 observations), and

239   cueing (auditory and visual) = 0 (72 observations). Three models were fitted as follows: Model

240   1: the independent variables were LDS-AP and LDS-ML (2 predictors); Model 2: the

241   independent variables were ACI 1-4, ACI 4-7, and ACI 7-10 for both the ML and AP directions

242   (6 predictors); and Model 3: the independent variables were α-ST, α-SL, and α-SS (3 predictors).

243   All α values were taken from Terrier (2016). The LASSO regularization factor was set via 10-

244   fold cross-validation. Receiver operating characteristic (ROC) curves were used to illustrate the

245   models' diagnostic abilities. Areas under the curves (AUCs), along with bootstrapped confidence

246   intervals, were computed as well (Fig. 6). Sensitivity and specificity were also evaluated

247   considering that the predicted class was 1 if the predicted probability was higher than 0.5. Fig. 7

248   presents the standardized coefficients of the multivariable logistic models, which indicate the

249   relative importance of each predictor.

250

251   **Results**

252   Divergence curves (Fig. 1) revealed a clear difference between cueing and no-cueing conditions,

253   especially for the AP signal. In the no-cueing condition (black curve), divergence increased

254   steadily, with moderate dampening. In contrast, for both auditory and visual cueing conditions,

255   dampening occurred more rapidly after four strides.

256   LDS and ACI are defined as slopes of the divergence curves measured at different intervals.

257   Given the dampening, it was expected that ACI measured further from the initial separation

258   would exhibit lower values. This was confirmed, as shown in the Fig. 3 boxplots: ACI 1-4 was

259 higher and more variable than either ACI 4-7 or ACI 7-10. Furthermore, the LDS, which was
260 computed during the first step, was larger (Fig. 2).
261   As shown by the effect size plots in Fig. 4, ACIs decreased strongly when individuals
262 followed auditory or visual cues. The effect was most pronounced for the AP signal, for which
263 both auditory and visual cueing had comparable effects. In contrast, a relevant difference existed
264 between auditory and visual cueing for the ML signals. Regarding LDS, the only significant
265 effect was between the auditory and no-cueing conditions in the ML directions (standardized
266 effect size: -0.38; 95% confidence interval: -0.69 – -0.04).
267   Fig. 5 shows the correlations among the LDS, ACI, and scaling exponents. Of particular note
268 is the high correlation found between ACI 4-7 measured by the ML direction and the scaling
269 exponents ($r = 0.86$ with α-ST, and $r = 0.86$ with α-SL). Other ACI spans exhibited weaker
270 correlations. ML-LDS was not correlated with other variables, while AP-LDS was weakly and
271 negatively correlated with scaling exponents ($r = -0.20$ with α-ST, and $r = -0.30$ with α-SS).
272   Using the ACIs and scaling exponents, multivariable logistic models differentiated very well
273 between the cueing and no-cueing conditions. The AUCs were close to 1 (α AUC = 0.996, ACI
274 AUC=0.973; Fig. 6). ACI model's sensitivity was 94%, and specificity was 89%. In contrast,
275 regarding LDS, the LASSO shrinkage procedure reduced the coefficients to zero, indicating a
276 non-significant model.
277   As shown in Fig. 7, The LASSO algorithm selected the most significant predictors, and no
278 important ones were set to 0. The LDS predictors are not shown, because all the coefficients
279 were null. The strongest predictors were α-ST and ACIs measured in the AP direction over long-
280 term spans (4-10).
281
Discussion
283 The aim of this study was to further explore whether ACI could be used to assess gait complexity
284 from continuous signals. The results strongly support the hypothesis that both DFA and ACI
285 measure the same thing: their values were strongly correlated, they both differed strongly
286 between the cueing and no-cueing conditions, and they both predicted cueing conditions with
287 high degrees of sensitivity and specificity. The results also show that ACI should be measured in
288 the AP direction and between four to seven strides downstream from the initial separation. In
289 addition, LDS seemed insensitive to cueing, further supporting its use as a pure gait stability
290 index.
291   A previous study assessed the effect of auditory cueing on stride-to-stride fluctuations in a
292 treadmill experiment among 20 young adults (Terrier & Dériaz, 2012). Scaling exponents of SL
293 and ST were strongly anti-persistent ($α < 0.5$) under the auditory cueing condition. Based on the
294 same data, another study investigated the effects of auditory cueing on LDS and ACI (Terrier &
295 Dériaz, 2013). ACI (still referred to as λ-L at that time) was computed over a timescale between
296 the 4th and 10th strides. The standardized effect size of the difference between the no-cueing and
297 auditory cueing conditions was -3.3 for both the AP and ML signals. In addition, a substantial
298 correlation between the scaling exponents and ACI was found (canonical correlation: $r = 0.83$).

299   Another research group also found similar results in a study that combined a foot-switch and an
300   accelerometer to evaluate overground walking (Sejdić et al., 2012); they found that both ACIs
301   (λ-LT) and scaling exponents were substantially lower when the walk was paced with a
302   metronome. The results of the present study confirm ACI's sensitivity to auditory cueing (effect
303   size < -2; Fig. 4). Overall, ACI seems sensitive to changes of long-range fluctuation patterns
304   induced by auditory sensorimotor synchronization.
305   The influence of visual cueing on ACI had not been previously studied. The present results
306   indicate that both visual and auditory cueing induced similar modifications to ACIs measured
307   from the AP signal (Figs. 1 and 4). Previous research has also demonstrated that visual and
308   auditory cueing have similar effects on scaling exponents (Terrier, 2016), which are incidentally
309   computed from the discretization of the AP signal. In contrast, the present study found that when
310   using ML measures, visual cueing had less of an effect than did auditory cueing (Fig. 4). It is
311   worth noting that the visual cueing procedure consisted of participants aiming their feet toward
312   rectangular visual targets (stepping stones). As a result, the task required voluntary leg control in
313   both the AP and ML directions. Further analyses are needed to specifically explore gait lateral
314   control under such circumstances, for instance by analyzing time series of step widths, which
315   would be computed from the discretization of the ML signal (see Terrier, 2012).
316   LDS and ACI are rates of divergence (i.e., slopes) computed from an average logarithmic
317   divergence curve (Fig. 1). Contrary to a real chaotic attractor, gait divergence curves do not
318   exhibit a linear region, from which the slope should be computed according to the Rosenstein
319   algorithm (Rosenstein, Collins & De Luca, 1993; Terrier & Dériaz, 2013). In fact, as illustrated
320   in Fig. 1, the divergence rate diminishes continuously along the curve. The determination of
321   range for computing ACI is therefore not straightforward. In their seminal researches, Dingwell
322   et al. computed the slope between the 4th and 10th strides, but without a clear justification for this
323   range (Dingwell et al., 2000; Dingwell & Cusumano, 2000). Subsequent studies followed
324   identical spans. However, based on an examination of the divergence curves, it may be
325   unnecessary to go that far from initial separation to estimate a meaningful long-term divergence,
326   especially since this also increases computational cost. For instance, it was recently shown that
327   an ACI (LDS-L) computed between the 2nd and 6th strides could discriminate between healthy
328   individuals and patients suffering chronic pain of lower limbs (Terrier et al., 2017). In addition,
329   the recent modeling study that introduced ACI observed that the ACI measured between the 2nd
330   and 4th strides was more responsive to the stride-to-stride noise structure than the ACI measured
331   between the 4th and the 10th strides, i.e., the originally proposed range (Terrier & Reynard, 2018).
332   Here, the results show that ACI 4-7 was superior to the other ranges: it exhibited the highest
333   correlation with the scaling exponents of ST and SL (r = 0.86 and 0.86; Fig. 5), it had the highest
334   contrast with the no-cueing condition (Fig. 4), and it was selected by the logistic model as the
335   second highest predictor of cueing conditions (standardized coefficient = 0.95; Fig. 7). In short, it
336   is very likely that it is not necessary to measure divergence after the 7th stride to assess ACI.
337   The results support the hypothesis that LDS and ACI measure different aspects of gait control.
338   Notably, LDS was not able to predict cueing conditions (not significant logistic model), and most

339   of the correlations between LDS and scaling exponents were weak (Fig. 5). The only significant
340   correlations concerned the AP-LDS and they were negative, i.e., went in opposite direction
341   compared to the ACI correlations. ML-LDS has been shown to be an index of gait instability
342   (Reynard et al., 2014) and fall risk (Bizovska et al., 2018). This may be due to the importance of
343   lateral stability for maintaining a steady and safe gait (Bauby & Kuo, 2000; Gafner et al., 2017).
344   The results of the present study support the use of ML-LDS for stability assessments given its
345   total independence from complexity measures (Fig. 5). However, it is unclear whether results
346   obtained from center-of-pressure trajectory are comparable to those obtained with other methods,
347   such as trunk accelerometry; incidentally, a large-scale accelerometry study found that AP-LDS
348   could predict future falls (van Schooten et al., 2015). The assumption that ML-LDS is better
349   suited for gait stability assessments thus requires further investigations. Overall, renaming long-
350   term LDS as ACI is further legitimated given the distinct responsiveness of short- and long-term
351   LDS to cueing.
352   The biggest strength of the present study is in its substantial number of strides measured in a
353   large sample of healthy adults (36), particularly when compared to other recent studies in the
354   field (Sejdić et al., 2012; Bohnsack-McLagan, Cusumano & Dingwell, 2016; Roerdink et al.,
355   2019). Evaluating gait complexity requires the analysis a large number of consecutive strides
356   (Marmelat & Meidinger, 2019). Similarly, reliability results show that many consecutive strides
357   are required to accurately assess ACI (Reynard & Terrier, 2014). As far as I know, LDS and ACI
358   have never been computed over a such large number of consecutive strides (500) so far.
359   Consequently, this study's findings most likely offer good generalizability.
360   The study's primary limitation is that the analyses of the center-of-pressure trajectories are
361   restricted to treadmill experiments with few potential applications. The center-of-pressure
362   approach has the advantage of allowing an easy discretization to compare both discrete time
363   series and continuous signals (Roerdink et al., 2008), but further investigations are required to
364   explore ACI potential in real-life applications using inertial sensors such as accelerometers.
365   Finally, it is important to underline that the use of ACI to assess the fluctuation structure of gait
366   is purely based on empirical considerations and has no clear theoretical support for now. Further
367   theoretical studies are required to investigate the relationship between scaling exponents and
368   ACI.
369
Conclusions
371   This study's findings support the hypothesis that ACI can provide information about the stride-
372   to-stride fluctuation structure of an individual's gait based on continuous signals. Given that ACI
373   fully harnesses continuous signals, it is not excluded that it requires fewer consecutive strides
374   than DFA for an accurate measurement, but this requires further studies. Accordingly,
375   information about gait complexity can be obtained while measuring a gait with inertial sensors,
376   such as accelerometers (Terrier et al., 2017; Terrier & Reynard, 2018).
377   ACI could thus assess the degree of motor control applied by walkers on their gait (the "thigh
378   control" hypothesis; see Dingwell & Cusumano [2010] and Roerdink et al. [2019]). A high ACI

379 would indicate an automated gait, while a lower ACI would be a sign of greater voluntary
380 attention dedicated to gait control. For example, it has been previously suggested that a low ACI
381 in patients with lower limb pain is due to enhanced gait control to avoid putting too much weight
382 on a painful leg (Terrier et al., 2017). Older studies that inappropriately used ACI as a gait
383 stability index should be reinterpreted with the "thigh control hypothesis" taken into account.
384 For example, Dingwell et al. found that patients suffering from peripheral neuropathy had lower
385 ACIs, which was interpreted as a higher gait stability obtained by lowering walking speed
386 (Dingwell et al., 2000). An alternative explanation would be that diminished sensory feedback
387 required more attention dedicated to gait control.
388   The use of LDS to characterize gait stability and assess fall risk has gained popularity over
389 recent years (Mochizuki & Aliberti, 2017; Bizovska et al., 2018; Mehdizadeh, 2018). Computing
390 ACI in addition to LDS can be made without further computation. Using ACI and LDS together
391 could be fruitful, as information about gait automaticity and cautiousness would complement
392 information about gait stability. It is hoped that the results of this study will help convince
393 researchers to reinstate the use of ACI to further enrich their gait analysis studies.
394

Acknowledgments

396 None

397

References

399 Almurad ZMH, Delignières D. 2016. Evenly spacing in Detrended Fluctuation Analysis. *Physica*
400   *A: Statistical Mechanics and its Applications* 451:63–69.
401   DOI:10.1016/j.physa.2015.12.155.
402 Almurad ZMH, Roume C, Blain H, Delignières D. 2018. Complexity Matching: Restoring the
403   Complexity of Locomotion in Older People Through Arm-in-Arm Walking. *Frontiers in*
404   *Physiology* 9. DOI: 10.3389/fphys.2018.01766.
405 Bauby CE, Kuo AD. 2000. Active control of lateral balance in human walking. *Journal of*
406   *Biomechanics* 33:1433–1440.
407 Bizovska L, Svoboda Z, Janura M, Bisi MC, Vuillerme N. 2018. Local dynamic stability during
408   gait for predicting falls in elderly people: A one-year prospective study. *PloS One*
409   13:e0197091. DOI: 10.1371/journal.pone.0197091.
410 Bohnsack-McLagan NK, Cusumano JP, Dingwell JB. 2016. Adaptability of stride-to-stride
411   control of stepping movements in human walking. *Journal of Biomechanics* 49:229–237.
412   DOI: 10.1016/j.jbiomech.2015.12.010.
413 Bruijn SM, Bregman DJJ, Meijer OG, Beek PJ, van Dieën JH. 2012. Maximum Lyapunov
414   exponents as predictors of global gait stability: a modelling approach. *Medical Engineering*
415   *& Physics* 34:428–436. DOI: 10.1016/j.medengphy.2011.07.024.
416 Bruijn SM, Meijer OG, Beek PJ, van Dieën JH. 2013. Assessing the stability of human
417   locomotion: a review of current measures. *Journal of the Royal Society, Interface*
418   10:20120999. DOI: 10.1098/rsif.2012.0999.
419 Chang MD, Sejdić E, Wright V, Chau T. 2010. Measures of dynamic stability: Detecting
420   differences between walking overground and on a compliant surface. *Human Movement*
421   *Science* 29:977–986. DOI: 10.1016/j.humov.2010.04.009.

422   Choi J-S, Kang D-W, Seo J-W, Tack G-R. 2017. Fractal fluctuations in spatiotemporal variables
423   when walking on a self-paced treadmill. *Journal of Biomechanics* 65:154–160. DOI:
424   10.1016/j.jbiomech.2017.10.015.
425   Delignières D, Torre K. 2009. Fractal dynamics of human gait: a reassessment of the 1996 data
426   of Hausdorff et al. *Journal of Applied Physiology (Bethesda, Md.: 1985)* 106:1272–1279.
427   DOI: 10.1152/japplphysiol.90757.2008.
428   Dingwell JB. 2006. Lyapunov Exponents. *Wiley Encyclopedia of Biomedical Engineering*.
429   Dingwell JB, Cusumano JP. 2000. Nonlinear time series analysis of normal and pathological
430   human walking. *Chaos (Woodbury, N.Y.)* 10:848–863. DOI: 10.1063/1.1324008.
431   Dingwell JB, Cusumano JP. 2010. Re-interpreting detrended fluctuation analyses of stride-to-
432   stride variability in human walking. *Gait & Posture* 32:348–353. DOI:
433   10.1016/j.gaitpost.2010.06.004.
434   Dingwell JB, Cusumano JP, Sternad D, Cavanagh PR. 2000. Slower speeds in patients with
435   diabetic neuropathy lead to improved local dynamic stability of continuous overground
436   walking. *Journal of Biomechanics* 33:1269–1277.
437   Fraser AM, Swinney HL. 1986. Independent coordinates for strange attractors from mutual
438   information. *Physical review. A, Atomic, molecular, and optical physics* 33:1134–1140.
439   DOI: 10.1103/PhysRevA.33.1134.
440   Gafner S, Bastiaenen C, Ferrari S, Gold G, Terrier P, Hilfiker R, Allet L. 2017. Hip muscle and
441   hand-grip strength to differentiate between older fallers and non-fallers: a cross-sectional
442   validity study. *Clinical interventions in aging* 13:1.
443   Goldberger AL, Amaral LAN, Hausdorff JM, Ivanov PC, Peng C-K, Stanley HE. 2002. Fractal
444   dynamics in physiology: alterations with disease and aging. *Proceedings of the National
445   Academy of Sciences of the United States of America* 99 Suppl 1:2466–2472. DOI:
446   10.1073/pnas.012579499.
447   González RC, López AM, Rodriguez-Uría J, Alvarez D, Alvarez JC. 2010. Real-time gait event
448   detection for normal subjects from lower trunk accelerations. *Gait & Posture* 31:322–325.
449   DOI: 10.1016/j.gaitpost.2009.11.014.
450   Hausdorff JM, Ladin Z, Wei JY. 1995. Footswitch system for measurement of the temporal
451   parameters of gait. *Journal of Biomechanics* 28:347–351.
452   Hausdorff JM, Peng CK, Ladin Z, Wei JY, Goldberger AL. 1995. Is walking a random walk?
453   Evidence for long-range correlations in stride interval of human gait. *Journal of Applied
454   Physiology (Bethesda, Md.: 1985)* 78:349–358. DOI: 10.1152/jappl.1995.78.1.349.
455   Holt KG, Jeng SF, Ratcliffe R, Hamill J. 1995. Energetic Cost and Stability during Human
456   Walking at the Preferred Stride Frequency. *Journal of Motor Behavior* 27:164–178. DOI:
457   10.1080/00222895.1995.9941708.
458   Kennel null, Brown null, Abarbanel null. 1992. Determining embedding dimension for phase-
459   space reconstruction using a geometrical construction. *Physical Review. A, Atomic,
460   Molecular, and Optical Physics* 45:3403–3411.
461   Lopez AM, Alvarez D, Gonzalez RC, Alvarez JC. 2008. Validity of four gait models to estimate
462   walked distance from vertical COG acceleration. *Journal of Applied Biomechanics*
463   24:360–367.
464   Marmelat V, Meidinger RL. 2019. Fractal analysis of gait in people with Parkinson's disease:
465   three minutes is not enough. *Gait & Posture* 70:229–234. DOI:
466   10.1016/j.gaitpost.2019.02.023.
467   McAndrew PM, Wilken JM, Dingwell JB. 2011. Dynamic stability of human walking in visually

468   and mechanically destabilizing environments. *Journal of Biomechanics* 44:644–649. DOI:
469   10.1016/j.jbiomech.2010.11.007.
470   Mehdizadeh S. 2018. The largest Lyapunov exponent of gait in young and elderly individuals: A
471   systematic review. *Gait & Posture* 60:241–250. DOI: 10.1016/j.gaitpost.2017.12.016.
472   Mochizuki L, Aliberti S. 2017. Gait Stability and Aging. In: Barbieri FA, Vitório R eds.
473   *Locomotion and Posture in Older Adults: The Role of Aging and Movement Disorders*.
474   Cham: Springer International Publishing, 45–54. DOI: 10.1007/978-3-319-48980-3_4.
475   Peng CK, Buldyrev SV, Goldberger AL, Havlin S, Mantegna RN, Simons M, Stanley HE. 1995.
476   Statistical properties of DNA sequences. *Physica A* 221:180–192.
477   Pereira APS, Marinho V, Gupta D, Magalhães F, Ayres C, Teixeira S. 2019. Music Therapy and
478   Dance as Gait Rehabilitation in Patients With Parkinson Disease: A Review of Evidence.
479   *Journal of Geriatric Psychiatry and Neurology* 32:49–56. DOI:
480   10.1177/0891988718819858.
481   Reynard F, Terrier P. 2014. Local dynamic stability of treadmill walking: intrasession and week-
482   to-week repeatability. *Journal of Biomechanics* 47:74–80. DOI:
483   10.1016/j.jbiomech.2013.10.011.
484   Reynard F, Vuadens P, Deriaz O, Terrier P. 2014. Could local dynamic stability serve as an early
485   predictor of falls in patients with moderate neurological gait disorders? A reliability and
486   comparison study in healthy individuals and in patients with paresis of the lower
487   extremities. *PLoS One* 9:e100550.
488   Riva F, Toebes MJP, Pijnappels M, Stagni R, van Dieën JH. 2013. Estimating fall risk with
489   inertial sensors using gait stability measures that do not require step detection. *Gait &*
490   *Posture* 38:170–174. DOI: 10.1016/j.gaitpost.2013.05.002.
491   Roerdink M, Coolen BH, Clairbois BHE, Lamoth CJC, Beek PJ. 2008. Online gait event
492   detection using a large force platform embedded in a treadmill. *Journal of Biomechanics*
493   41:2628–2632. DOI: 10.1016/j.jbiomech.2008.06.023.
494   Roerdink M, Daffertshofer A, Marmelat V, Beek PJ. 2015. How to Sync to the Beat of a
495   Persistent Fractal Metronome without Falling Off the Treadmill? *PloS One* 10:e0134148.
496   DOI: 10.1371/journal.pone.0134148.
497   Roerdink M, de Jonge CP, Smid LM, Daffertshofer A. 2019. Tightening Up the Control of
498   Treadmill Walking: Effects of Maneuverability Range and Acoustic Pacing on Stride-to-
499   Stride Fluctuations. *Frontiers in Physiology* 10. DOI: 10.3389/fphys.2019.00257.
500   Rosenstein MT, Collins JJ, De Luca CJ. 1993. A practical method for calculating largest
501   Lyapunov exponents from small data sets. *Physica D: Nonlinear Phenomena* 65:117–134.
502   DOI: 10.1016/0167-2789(93)90009-P.
503   van Schooten KS, Pijnappels M, Rispens SM, Elders PJM, Lips P, van Dieën JH. 2015.
504   Ambulatory fall-risk assessment: amount and quality of daily-life gait predict falls in older
505   adults. *The Journals of Gerontology. Series A, Biological Sciences and Medical Sciences*
506   70:608–615. DOI: 10.1093/gerona/glu225.
507   van Schooten KS, Sloot LH, Bruijn SM, Kingma H, Meijer OG, Pijnappels M, van Dieën JH.
508   2011. Sensitivity of trunk variability and stability measures to balance impairments
509   induced by galvanic vestibular stimulation during gait. *Gait & Posture* 33:656–660. DOI:
510   10.1016/j.gaitpost.2011.02.017.
511   Sejdić E, Fu Y, Pak A, Fairley JA, Chau T. 2012. The effects of rhythmic sensory cues on the
512   temporal dynamics of human gait. *PloS One* 7:e43104. DOI:
513   10.1371/journal.pone.0043104.

514 Su JL-S, Dingwell JB. 2007. Dynamic stability of passive dynamic walking on an irregular
515   surface. *Journal of Biomechanical Engineering* 129:802–810. DOI: 10.1115/1.2800760.
516 Takens F. 1981. Detecting strange attractors in turbulence. In: Rand D, Young L-S eds.
517   *Dynamical Systems and Turbulence, Warwick 1980*. Lecture Notes in Mathematics.
518   Springer Berlin Heidelberg, 366–381.
519 Terrier P. 2012. Step-to-step variability in treadmill walking: influence of rhythmic auditory
520   cueing. *PloS One* 7:e47171. DOI: 10.1371/journal.pone.0047171.
521 Terrier P. 2016. Fractal Fluctuations in Human Walking: Comparison Between Auditory and
522   Visually Guided Stepping. *Annals of Biomedical Engineering* 44:2785–2793. DOI:
523   10.1007/s10439-016-1573-y.
524 Terrier P, Carré JL, Connaissa M, Léger B, Luthi F. 2017. Monitoring of Gait Quality in Patients
525   With Chronic Pain of Lower Limbs. *IEEE Transactions on Neural Systems and
526   Rehabilitation Engineering* 25:1843–1852. DOI: 10.1109/TNSRE.2017.2688485.
527 Terrier P, Dériaz O. 2011. Kinematic variability, fractal dynamics and local dynamic stability of
528   treadmill walking. *Journal of NeuroEngineering and Rehabilitation* 8:12.
529 Terrier P, Dériaz O. 2012. Persistent and anti-persistent pattern in stride-to-stride variability of
530   treadmill walking: influence of rhythmic auditory cueing. *Human movement science*
531   31:1585–1597.
532 Terrier P, Dériaz O. 2013. Non-linear dynamics of human locomotion: effects of rhythmic
533   auditory cueing on local dynamic stability. *Frontiers in physiology* 4:230.
534 Terrier P, Reynard F. 2015. Effect of age on the variability and stability of gait: a cross-sectional
535   treadmill study in healthy individuals between 20 and 69 years of age. *Gait & posture*
536   41:170–174.
537 Terrier P, Reynard F. 2018. Maximum Lyapunov exponent revisited: Long-term attractor
538   divergence of gait dynamics is highly sensitive to the noise structure of stride intervals.
539   *Gait & Posture* 66:236–241. DOI: 10.1016/j.gaitpost.2018.08.010.
540 Terrier P, Schutz Y. 2005. How useful is satellite positioning system (GPS) to track gait
541   parameters? A review. *Journal of neuroengineering and rehabilitation* 2:28.
542 Terrier P, Turner V, Schutz Y. 2005. GPS analysis of human locomotion: further evidence for
543   long-range correlations in stride-to-stride fluctuations of gait parameters. *Human
544   movement science* 24:97–115.
545 Tibshirani R. 1996. Regression Shrinkage and Selection Via the Lasso. *Journal of the Royal
546   Statistical Society: Series B (Methodological)* 58:267–288. DOI: 10.1111/j.2517-
547   6161.1996.tb02080.x.
548 West BJ. 2013. *Fractal physiology and chaos in medicine*. New Jersey: World Scientific.
549 Yoo GE, Kim SJ. 2016. Rhythmic Auditory Cueing in Motor Rehabilitation for Stroke Patients:
550   Systematic Review and Meta-Analysis. *Journal of Music Therapy* 53:149–177. DOI:
551   10.1093/jmt/thw003.
552

Table 1: Descriptive statistics of the attractor complexity index (ACI)

Means and standard deviations (SD) of ACI measured in the 36 subjects under the three experimental conditions. AP: anteroposterior. ML: mediolateral.

N=36	ACI 1-4				ACI 4-7				ACI 7-10			
ACI x 1000	AP		ML		AP		ML		AP		ML	
	mean	SD	mean	SD	mean	SD	mean	SD	mean	SD	mean	SD
No cueing	2.16	(0.34)	1.39	(0.30)	0.87	(0.12)	0.51	(0.19)	0.47	(0.12)	0.36	(0.11)
Auditory cueing	1.78	(0.37)	1.21	(0.26)	0.50	(0.19)	0.20	(0.11)	0.21	(0.13)	0.08	(0.09)
Visual cueing	1.68	(0.52)	1.20	(0.29)	0.43	(0.22)	0.32	(0.19)	0.16	(0.13)	0.16	(0.14)

Figure 1

Figure 1: Divergence curves

Using time-delay embedding, 5-dimensional attractors were reconstructed from the anteroposterior and mediolateral coordinates of a center-of-pressure trajectory. The logarithmic divergence from neighbor trajectories (y-axis) was averaged across trajectories and participants (N=36), and drawn against normalized time (strides, x-axis). Three curves are shown, one for each experimental condition.
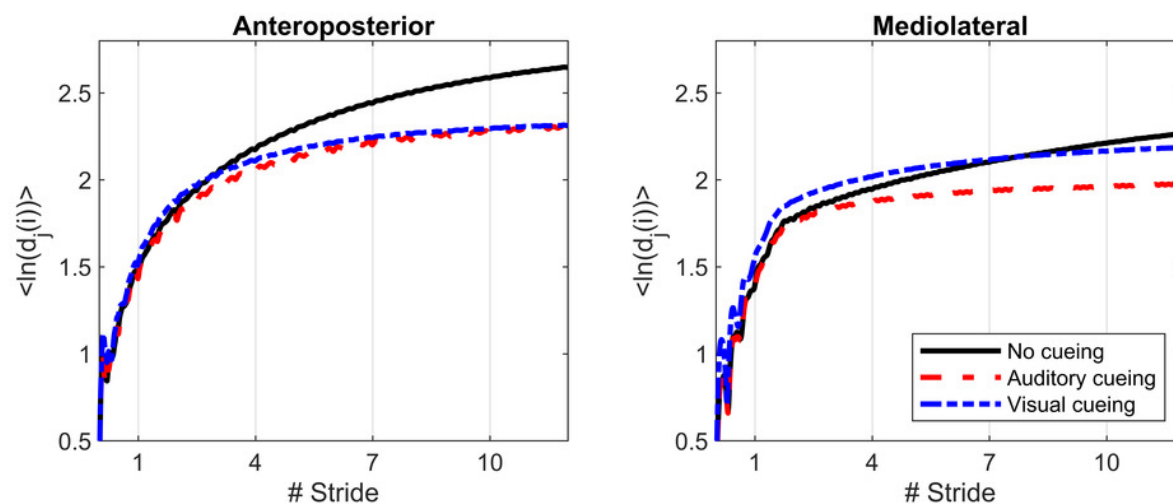
Figure 2

Figure 2: Descriptive statistics of the local dynamic stability (LDS)

The notched boxplots summarize the distribution of individual results (N = 36) across the three experimental conditions for the anteroposterior (A) and the mediolateral (B) signals. The notch extremes correspond to the 95% confidence intervals of the medians. The red + symbols indicate outliers.
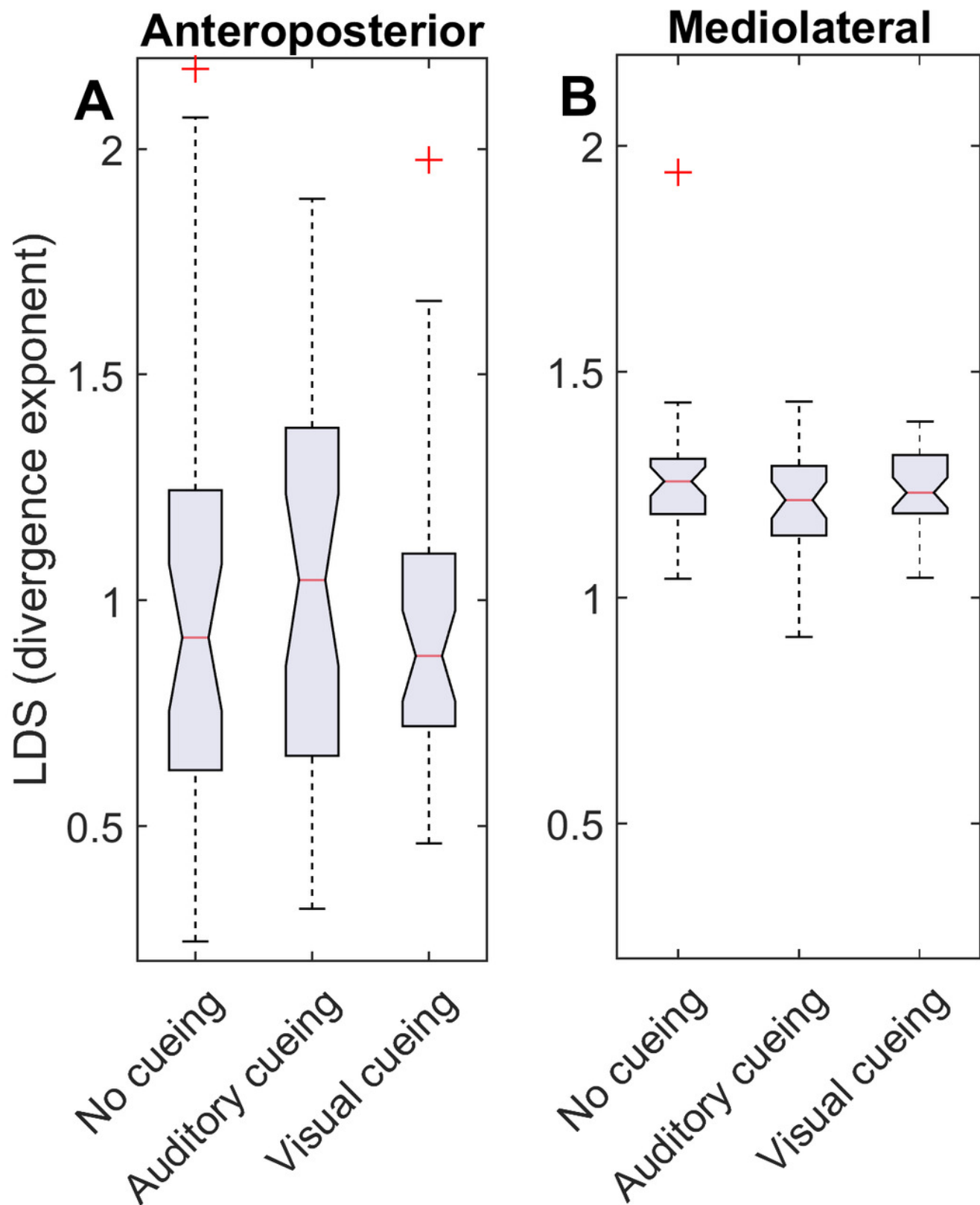
Figure 3

Figure 3: Descriptive statistics of the attractor complexity index (ACI)

The notched boxplots summarize the distribution of individual results (N = 36) across the three experimental conditions for the three different ACI spans, and for the anteroposterior (A) and the mediolateral (B) signals. The notch extremes correspond to the 95% confidence intervals of the medians. The red + symbols indicate outliers.
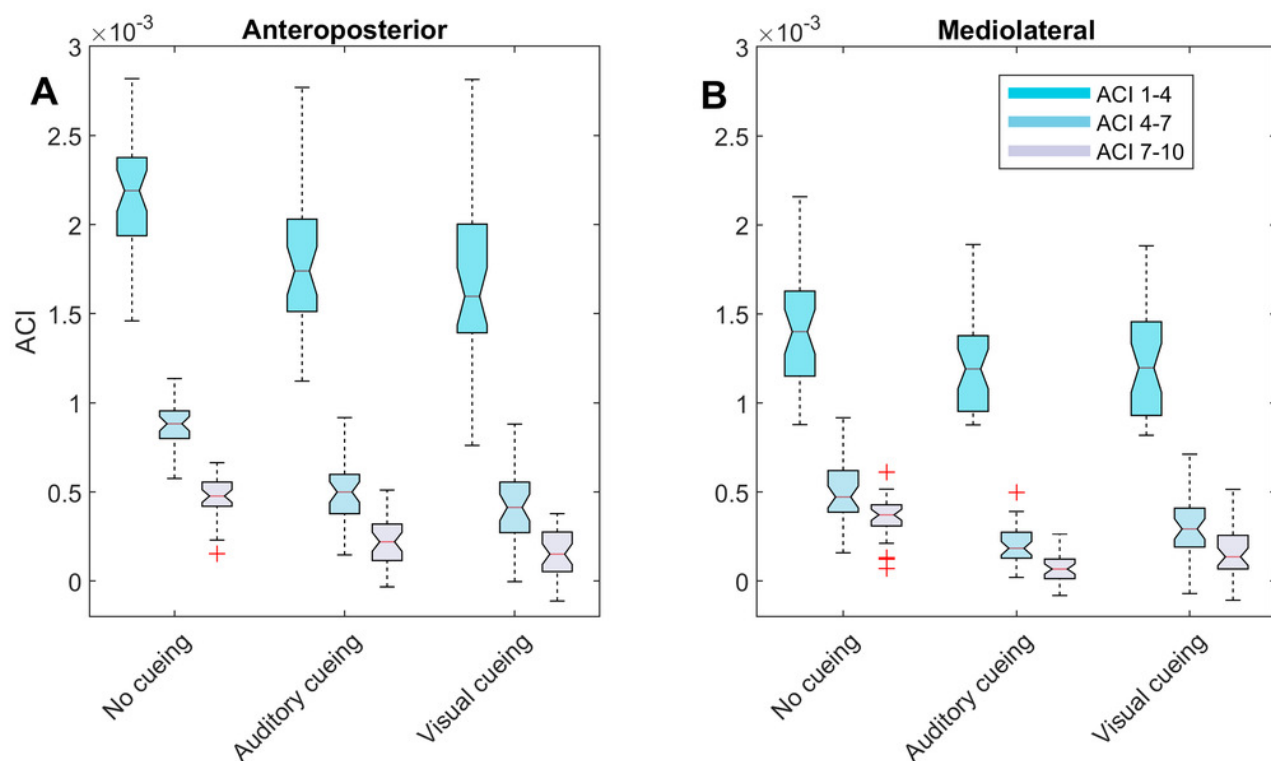
Figure 4

Figure 4: Effect sizes of attractor complexity index (ACI)

Standardized effect size (Hedges' g) of the difference between cueing and no-cueing conditions for the anteroposterior (A) and the mediolateral signals (B). Vertical lines are 95% confidence intervals (Bonferroni corrected). AC: auditory cueing; VC: visual cueing; NC: no-cueing.
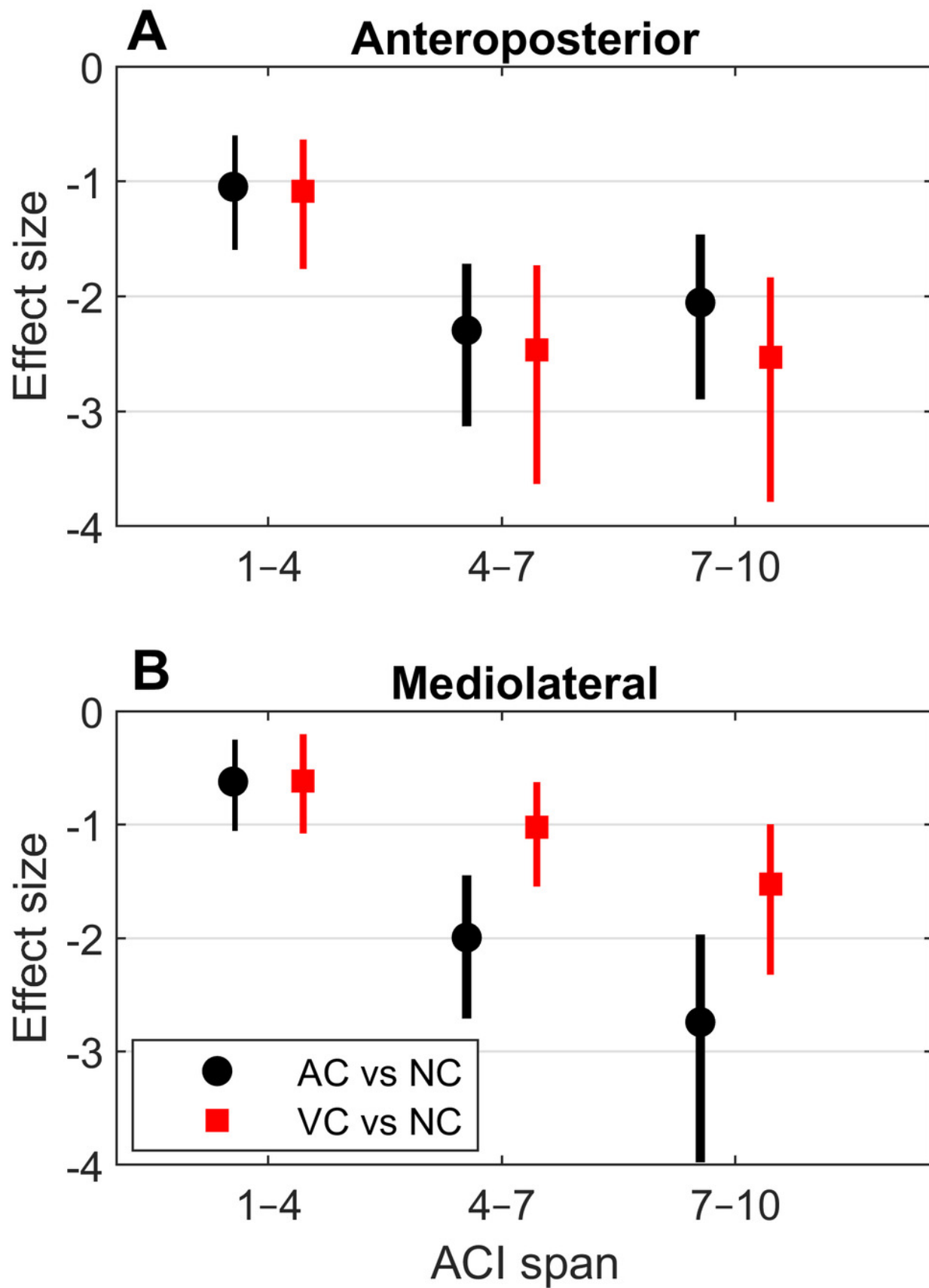
Figure 5: Correlations and scatter plots across local dynamic stability (LDS), attractor complexity index (ACI), and scaling exponent (alpha) measures

Pearson's correlation coefficients (r) are shown on the lower left. Bold values indicate significant results for the hypothesis test for $r = 0$. In the upper right, scatter plots with the linear fits are shown. AP: anteroposterior; ML: mediolateral; ST: stride time; SL: stride length; SS: stride speed.
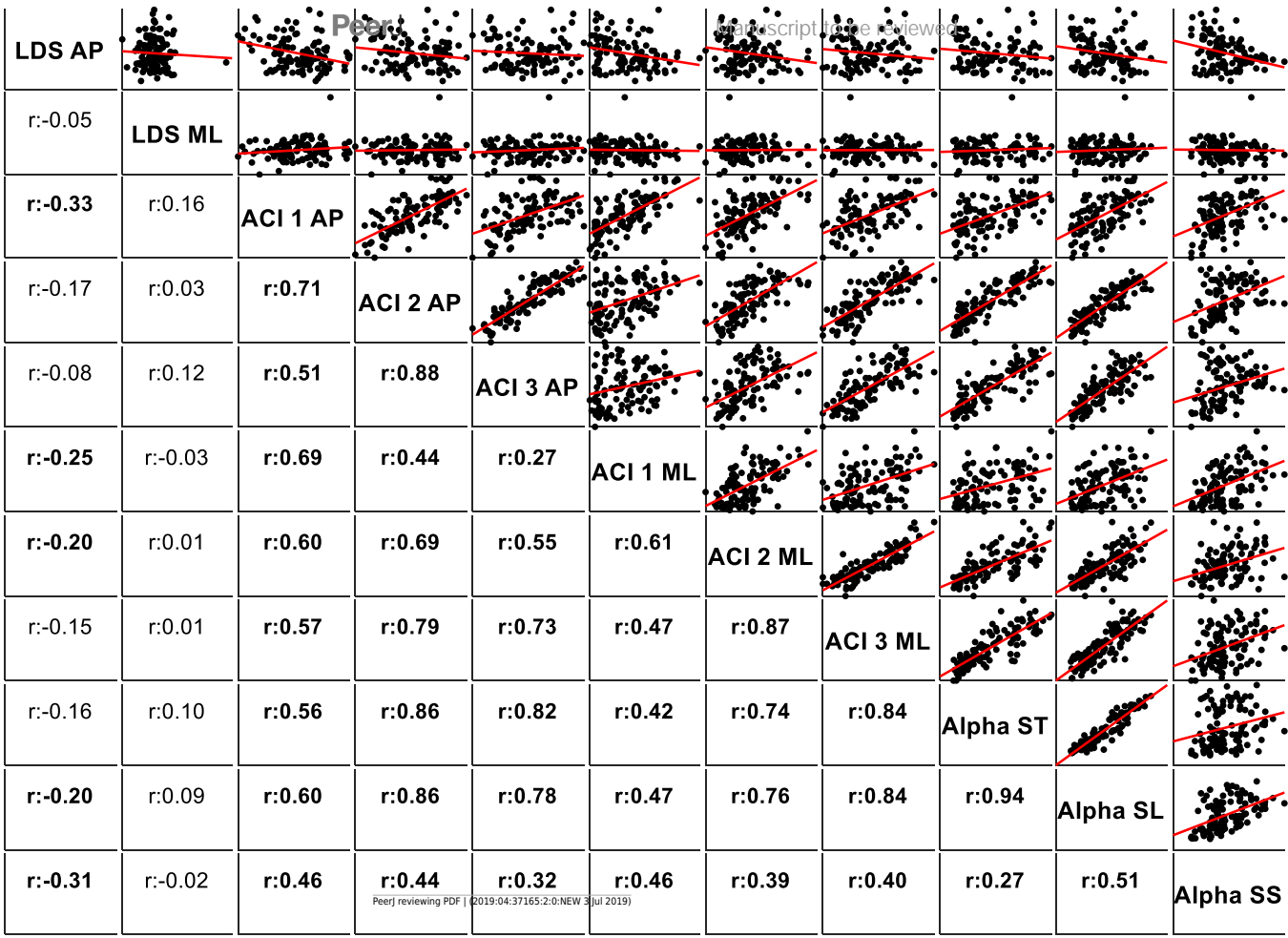
Figure 6

Figure 6: Receiver operating characteristic (ROC) curves

ROC curves for two multivariable logistic models predicting cueing/no-cueing conditions: 1) scaling exponent (alpha); and 2) attractor complexity index (ACI). Areas under the curves (AUCs) are written with their confidence intervals.
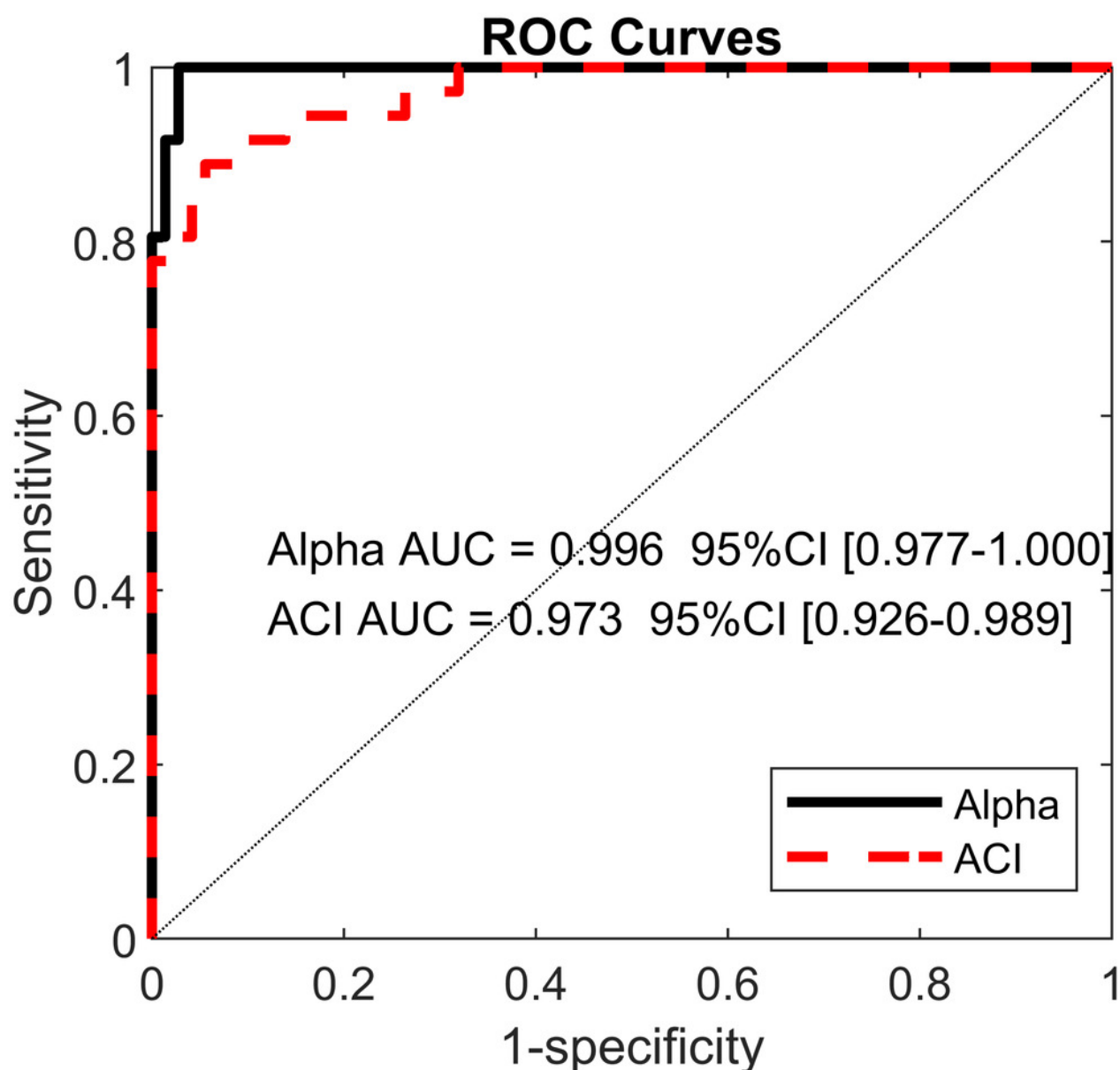
Figure 7

Figure 7: Standardized coefficients of the multivariable logistic models

Two multivariable logistic models were fitted using: (A) scaling exponents (Alphas); and (B) attractor complexity indexes (ACIs). A least absolute shrinkage and selection operator (LASSO) was used to regularize fitting. Bars show the value of the standardized beta coefficient of the logistic regressions for each predictor. AP: anteroposterior; ML: mediolateral; ST: stride time; SL: stride length; SS: stride speed.